J Solid State Electrochem (2001) 5: 23–28 

ORIGINAL PAPER

Shu G. Zhang · Yasutaka Hara · Seijiro Suda
Tsutomu Morikawa · Hiroshi Inoue · Chiaki Iwakura

# Physicochemical and electrochemical hydriding–dehydriding characteristics of amorphous $MgNi_x$ ($x = 1.0, 1.5, 2.0$) alloys prepared by mechanical alloying

Received: 28 August 1999 / Accepted: 23 November 1999

**Abstract** Physicochemical and electrochemical hydriding-dehydriding characteristics of amorphous $MgNi_x$ ($x = 1.0$, 1.5, 2.0) alloys prepared by mechanical alloying have been investigated. It was found that the increase of Ni content in the alloys resulted in greatly enhanced kinetics for both absorption and desorption of hydrogen, while the saturation capacity showed the reverse tendency. Charge–discharge tests showed that the increase in Ni content lead to a significant enhancement in cycle performance of $MgNi_x$ alloy electrodes. X-ray photoelectron spectroscopic and X-ray excited Auger electron spectroscopic investigations indicated the existence of a significantly thicker Ni-enriched layer for the $MgNi_{1.5}$ and $MgNi_{2.0}$ alloys than for the MgNi alloy. These results reveal that excess of Ni in $MgNi_x$ alloys may improve the cycle performance of alloy electrodes by suppressing the segregation of Mg during electrochemical cycling, and the Ni in the topmost surface layer is mainly responsible for the improvement in the kinetics of hydrogen absorption.

**Key words** Magnesium–nickel alloys · Mechanical alloying · Hydriding–dehydriding kinetics · X-ray photoelectron spectroscopy

## Introduction

From the point of view of reaching a high energy density, lightweight elements such as magnesium and carbon have attracted a great deal of interest for hydrogen storage purposes. Carbon nanocubes [1] or fibers [2] were reported to be able to store a large amount of hydrogen, but high pressure was needed for hydrogen absorption. Metallic Mg and crystalline Mg-based alloys could only reversibly absorb and desorb hydrogen at high temperatures, such as 250 °C for $Mg_2Ni$ and higher temperatures for metallic Mg, at around atmospheric pressure [3]. Recently, many groups have therefore concentrated their research activities on lowering the hydriding temperature of Mg-based alloys.

Lei et al. [4] reported that a MgNi alloy prepared by ball-milling can be charged and discharged in a nickel-metal hydride battery at room temperature, which opened a new possibility for the application of Mg-based alloys in nickel-metal hydride batteries. Our group [5, 14] found that a composite of MgNi alloy with graphite resulted in a greatly enhanced electrode performance. Orimo and Fujii [6] reported that by ball-milling of $Mg_2Ni$ with Ni powder, the resulting MgNi alloy absorbed hydrogen more easily than the initial crystalline $Mg_2Ni$ alloy. Kohno and Kanda [7] and our group [8, 9] reported that amorphous alloys prepared by ball-milling of $Mg_2Ni$ with Ni powder exhibited discharge capacities ranging from 750 to 1086 mAh $g^{-1}$ ($Mg_2Ni$). All the investigations suggest that the amorphous Mg-based alloys differ greatly in nature from the crystalline ones, and Ni may play an extremely important role of facilitating the absorption and desorption of hydrogen.

On the other hand, although amorphous MgNi alloys prepared by mechanical alloying have been demonstrated to absorb and desorb hydrogen reversibly at room temperature, the cycle performance of the alloy electrodes was very poor. Some attempts have been made to substitute either Mg or Ni in MgNi with foreign metals for an improvement in the electrode performance of the MgNi alloy [10, 11]. In order to evaluate the effect resulting from the foreign metals, it is vitally important to understand how an individual element in an alloy influences the overall hydrogen absorption properties. On the other hand, although the amorphous $LaNi_5$ alloy

S.G. Zhang · Y. Hara · H. Inoue · C. Iwakura (✉)
Department of Applied Chemistry,
Osaka Prefecture University, Sakai,
Osaka 599-8531, Japan

S. Suda
Department of Chemical Engineering,
Kogakuin University, Hachioji,
Tokyo 192-0015, Japan

T. Morikawa
Technology Research Institute of Osaka Prefecture,
Izumi, Osaka 594-1157, Japan

was shown to have a similar short-range order as its crystalline counterpart [12], there has been little information on the hydrogen absorption sites in the amorphous MgNi alloy, because a crystalline MgNi alloy is unavailable [13]. Investigations on the effect of Ni on the electrochemical behavior of MgNi alloys as well as the relation between the structural characteristics and the electrochemical hydriding properties will help in understanding the electrode performance of Mg-based alloys.

With the above in mind, in this work, $MgNi_x$ alloys have been investigated with the intention of obtaining insight into the role of Ni and the hydrogen absorption sites in $MgNi_x$ alloys.

## Experimental

$MgNi_x$ alloys were prepared by ball-milling the mixtures of metallic Mg (99.99%, 100 mesh, Aldrich) and Ni (99%, 50 mesh, Aldrich) powders using a high-energy ball-mill (Fritsch P7). The metallic powders were first mixed in a mortar for several tens of minutes and then the resulting mixture was ball-milled for a certain time. The detailed preparation procedures have been given elsewhere [14, 15]. The prepared alloys were kept in an Ar atmosphere with residual air pressure less than $10^{-2}$ Torr for the spectroscopic measurements or hydrogen absorption tests. The absorption kinetics of hydrogen and the P-C-T curves for the $MgNi_x$ alloy-hydrogen systems were measured with a Sievert-type apparatus. For preparation of the electrodes, alloy powder was mixed with Cu powder in a weight ratio of 1:3, and 0.4 g of the mixture was pressed under a pressure of 10 t at room temperature for 1 min. Finally, the pellet was covered with a sheet of Ni mesh and soldered to a Ni wire. In charge–discharge cycle tests, the negative electrode was charged at 100 mA/g and discharged to −0.6 V vs. Hg/HgO at 50 mA/g. After every charging, the circuit was opened for 10 min. Other details of the preparation of the alloy electrodes and charge–discharge tests were performed according to the same procedures as those described in our previous paper [8].

X-ray photoelectron spectroscopy (XPS) and X-ray excited Auger electron spectroscopy (XAES) measurements were carried out with a PHI ESCA 5700 CI spectrometer using Al $K_\alpha$ radiation (1486.6 eV). $Ar^+$ ion bombardment at 4 keV was used for depth profile measurements and the sputtering rate, estimated using $SiO_2$/Si as a reference, was about 30 Å/min. The C 1s peak of the adsorbed carbon at 284.6 eV was used to calibrate the peak positions. The quantitative data were obtained using a sensitive factor correction. The Ni/Mg ratios were estimated from the Ni 2p and Mg 2p peaks. Before each measurement, the brief exposure to air was strictly controlled to be the same from sample to sample, which was comparable well with the histories of the alloy electrodes for the electrochemical experiments.

## Results and discussion

Figure 1 shows the X-ray diffraction (XRD) patterns of the $MgNi_x$ alloys. Similarly to MgNi alloy, the $MgNi_{1.5}$ and $MgNi_{2.0}$ alloys showed broad halos in their XRD profiles. The halo shifts to a higher $2\theta$ value as the Ni content increases from MgNi to $MgNi_{1.5}$ and $MgNi_{2.0}$. A reduction in the average atomic distance in the alloys has been caused by the introduction of Ni, which has a smaller radius than Mg. As has been reported for the MgNi alloy, such a XRD pattern corresponds to a halo in electron diffraction measurement [16]; thus the alloys studied here are all amorphous in structure.

Figure 2 depicts the time course of the amount of absorbed hydrogen for the $MgNi_x$ alloys. More rapid absorption of hydrogen was observed for the $MgNi_{1.5}$ and $MgNi_{2.0}$ alloys, as compared with that for the MgNi alloy. The time to reach the maximal H/M value was about 50 min for $MgNi_2$, 100 min for $MgNi_{1.5}$, and 500 min for the MgNi alloy. Obviously, the kinetics of hydrogen absorption were greatly improved by the introduction of excess Ni.

On the other hand, in spite of the increase in hydrogen absorption kinetics, the saturation capacity of hydrogen absorption into the alloys decreased in the order MgNi > $MgNi_{1.5}$ > $MgNi_{2.0}$, i.e., as the mole fraction of Mg in the alloys decreased. For MgNi, the saturation capacity described as a H/M ratio is ca. 1.0, while for $MgNi_{1.5}$ and $MgNi_{2.0}$ the H/M ratios are 0.8 and 0.6, respectively. It is particularly interesting to note that the opposite tendency was observed for the absorption kinetics and the saturation absorption capacity.

As demonstrated previously, thermogravimetric analysis (TGA) is one of the useful tools to monitor the

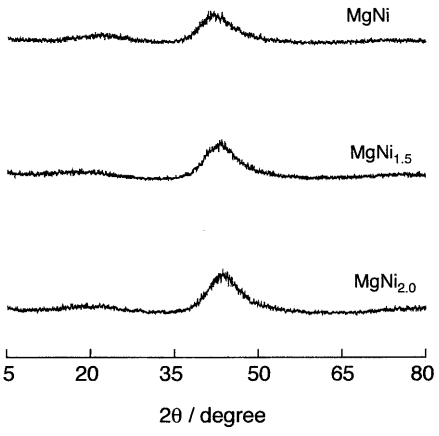


**Fig. 1** X-ray diffraction patterns of the $MgNi_{1.5}$ and $MgNi_{2.0}$ alloys

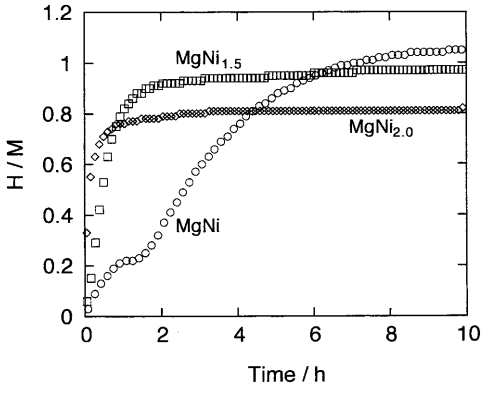


**Fig. 2** Time course of the amount of absorbed hydrogen for the $MgNi_x$ alloys

hydrogen desorption characteristics of a hydrided alloy. Figure 3 shows the TGA curves for hydrided $MgNi_x$ alloys. The weight loss for hydrided MgNi started at around 210 °C, while that for $MgNi_{1.5}$ and $MgNi_{2.0}$ started at temperatures lower than 80 °C. The desorption process was complete at 300 °C for MgNi, at 220 °C for $MgNi_{1.5}$, and at 200 °C for $MgNi_2$. A marked lowering in the desorption temperature together with the end temperature for hydrogen desorption were observed with an increase in Ni content in the $MgNi_x$ alloys. The maxima of the weight loss, which corresponds to the hydrogen absorption capacity of the alloys, are about 2.0 wt%, 1.1 wt%, and 0.7 wt% for MgNi, $MgNi_{1.5}$, and $MgNi_{2.0}$, respectively.

For all the three kinds of alloys, similar P-C isotherms were observed, which did not show any plateau-like trace under the experimental conditions, typical for amorphous alloys. This result reveals that the $MgNi_x$ alloys with $x = 1.0$–$2.0$ have no substantial difference in their long-range order structure, all being of amorphous character. TGA and PCT measurements revealed identical phenomena, i.e., the increase in Ni content in the alloy facilitated the absorption and desorption but resulted in a decrease in hydrogen absorption capacity of the alloys. It is expected that an improvement in the kinetics should result in an enhanced efficiency of hydrogen absorption in the alloy, but the above facts indicate that the real location sites for hydrogen in MgNi, $MgNi_{1.5}$, and $MgNi_{2.0}$ alloys may be principally related by the Mg sites in the alloys. A change in the Ni content in the alloys only resulted in a different dispersion level of Mg, i.e., a higher dispersion level contributed to higher absorption kinetics, while the decrease in capacity was due to the decrease in Mg/(Mg + Ni) in the alloys.

The present cases are quite different from that for the $Mg_2Ni$ alloy. For $Mg_2Ni$, by addition of Ni and upon ball-milling, not only enhanced kinetics but also a continuous increase in the absorption capacity of hydrogen were observed [9]. The effect of Ni may be mainly structural, such as Ni can induce the amorphization of $Mg_2Ni$ alloy during ball-milling. Although it cannot be clearly stated which is the key factor for the structural change and the catalytic effect of Ni in the $Mg_2Ni$-Ni system, it is most likely that the location sites for hydrogen have been changed during the introduction of Ni into $Mg_2Ni$.

For metallic Mg, addition of Ni could cause a great improvement in the kinetics of hydrogen absorption together with a decrease in capacity [17]. For hydrogen absorption, the first step has been proposed to be that molecular hydrogen is dissociated into atomic H, which is followed by the migration of atomic H into the bulk of the alloy. Ni is one of the most powerful metals to catalyze the dissociation of molecular $H_2$. The decrease in the absorption capacity of hydrogen upon increasing the Ni content is most likely to be due to the dilution of the real hydrogen absorbing sites in $MgNi_x$ alloys. The possibility cannot be excluded that the hydrogen absorbing sites in the $MgNi_x$ alloys are just the metallic Mg sites diluted in metallic Ni, which can more effectively absorb hydrogen than pure metallic Mg owing to decrease of the particle sizes and the excellent catalytic effect of Ni.

Figure 4 depicts the charge–discharge capacities as a function of the cycle number for the $MgNi_x$ alloys. For all the $MgNi_x$ alloys with $x = 1.0$–$2.0$, the largest discharge capacity was obtained at the first cycle, indicating that the fundamental structural characteristics of the three alloys corresponding to the activation and hydriding processes may be quite similar. In the case of MgNi, comparable with the previously reported values [4, 10], the maximum discharge capacity amounts to about 490 mAh $g^{-1}$, while $MgNi_{1.5}$ and $MgNi_{2.0}$ have a discharge capacities of 370 mAh $g^{-1}$ and 200 mAh $g^{-1}$, respectively. A monotonous decrease in the discharge capacity was observed from MgNi to $MgNi_{2.0}$ for the first cycle. This may be attributed to the decrease of the Mg amount in a unit mass of the alloy, and also suggests that Ni in alloys contributes little to the discharge capacity of $MgNi_x$ directly.

Also from Fig. 4, another interesting feature that can be seen is that the cycle performance of either the

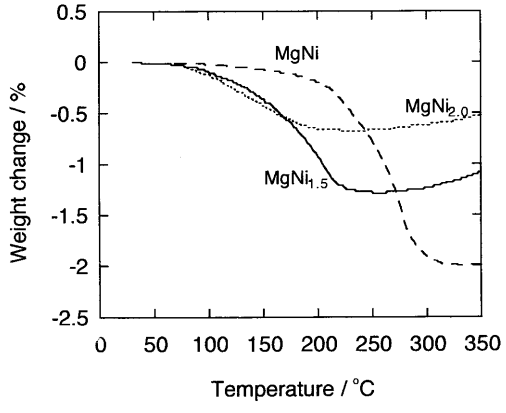


**Fig. 3** Thermogravimetric analysis curves for the hydrided $MgNi_x$ alloys

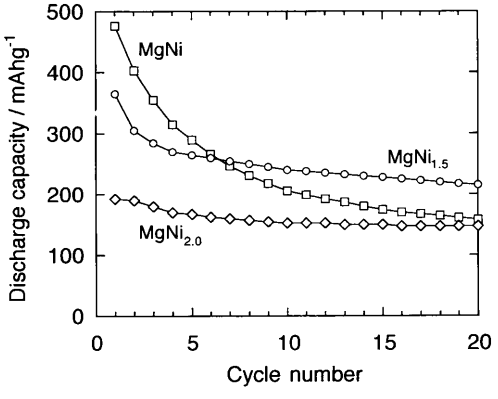


**Fig. 4** Discharge capacity as a function of the cycle number for the $MgNi_x$ alloys

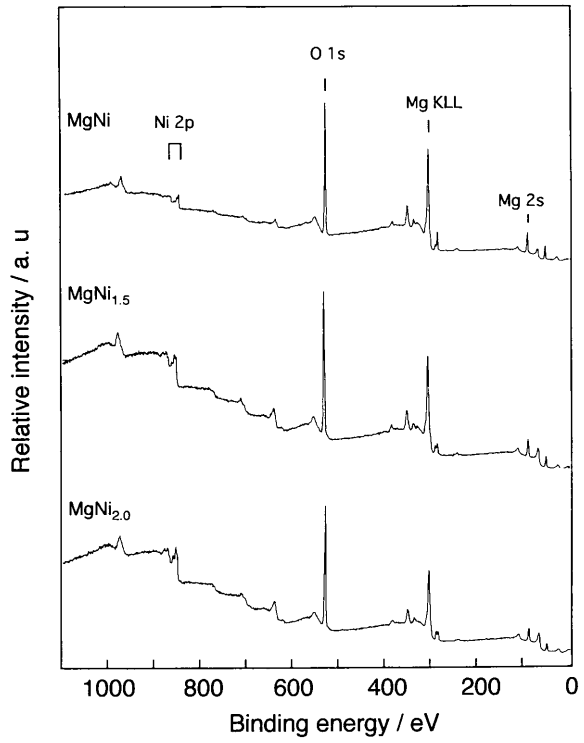


**Fig. 5** Wide-scan X-ray photoelectron spectra (XPS) observed for the $MgNi_x$ alloys

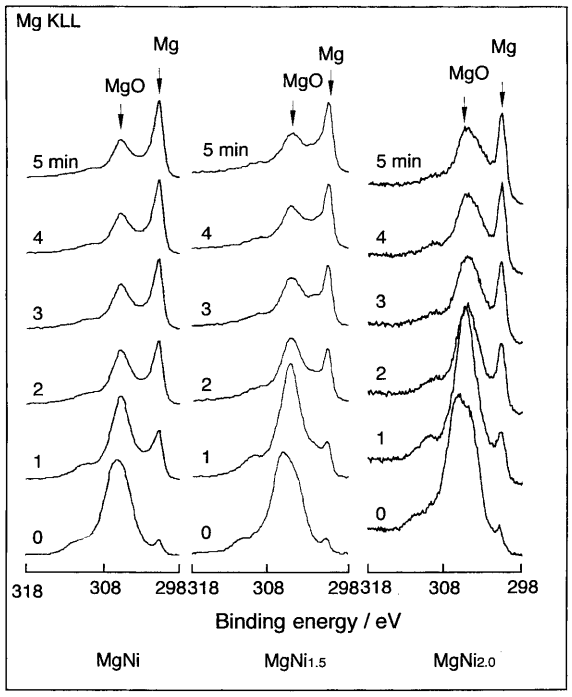


**Fig. 6** Change of Mg KLL X-ray excited Auger electron spectra of $MgNi_x$ alloys during sputtering

$MgNi_{1.5}$ or the $MgNi_{2.0}$ alloy is much better than the MgNi alloy. For the $MgNi_{1.5}$ alloy, although the difference in discharge capacity from that of the MgNi alloy at the first cycle amounts to 120 mAh $g^{-1}$, a discharge capacity the same as that of the MgNi alloy was reached at the sixth cycle, and a higher level than MgNi alloy was kept afterwards. At the 20th cycle, the $MgNi_{1.5}$ alloy exhibited a discharge capacity of 210 mAh $g^{-1}$, which was about 60 mAh $g^{-1}$, higher than that of the MgNi alloy. In the case of the $MgNi_{2.0}$, even though the difference in discharge capacity from that of the MgNi alloy was much larger at the first cycle, a similar discharge capacity to the MgNi alloy was observed at the 20th cycle. All these results suggest that the cycle life of $MgNi_x$ alloy electrodes can be greatly enhanced by increasing the Ni content.

In order to understand the role played by Ni in $MgNi_x$ alloy electrodes, the $MgNi_x$ alloys were investigated by XPS and XAES. Figure 5 shows the wide-scan XPS spectra of $MgNi_x$ alloys. Strong Mg KLL, Mg 2s, and O 1s peaks and a weak Ni 2p peak can be clearly observed for all three alloys, revealing that their surface contaminants were quite similar and that the alloy surfaces were oxidized to a certain extent. In a previous work [15], we have noticed that Mg can protect Ni from oxidation in alloys owing to the larger oxidation affinity of Mg towards oxygen. Thus, it is expected that the surface oxygen observed in the wide-scan XPS spectra may be mainly attached to Mg.

Figure 6 shows the Mg KLL XAES spectra observed with various $MgNi_x$ alloys during $Ar^+$ sputtering. It has been found that XAES measurements are a very useful method in distinguishing the metallic Mg from its oxide counterpart, owing to the larger chemical shift in XAES than XPS [15]. For all three alloys, the band at around 301 eV can be assigned to metallic Mg and the one at around 305 eV to magnesium oxide [18]. For all three alloys, MgO dominates and only a small amount of Mg occurs in the metallic state at the alloy surface. A decrease in the amount of MgO was observed upon sputtering and, at a certain depth of the alloy bulk, metallic Mg becomes dominant. Minor differences in the full width at half maximum (FWHM) of Mg KLL bands for alloys with different $x$ values were most probably due to minor changes in the surface contamination. These results indicated that the chemical state of Mg is similar for all three alloys, and therefore the difference in the cycle performance of the $MgNi_x$ alloy electrodes did not result from any difference in the chemical state of Mg directly.

Figure 7 shows the Ni 2p core level spectra of $MgNi_x$ alloys during sputtering. The set of bands appearing at 852.5 and 870.0 eV correspond to the metallic nickel and the other set of peaks at 855.0 and 875.2 eV are related to nickel oxide, respectively [19]. Before sputtering, the intensity of the Ni 2p peaks are very weak, indicating the small amount of Ni at the alloy surface. The peaks for metallic Ni 2p for MgNi are much stronger those that for NiO, which clearly indicates that Ni mainly exists in the metallic state with only a small fraction of NiO existing on the surface of the MgNi alloy. In the cases of $MgNi_{1.5}$ and $MgNi_{2.0}$, the peaks due to NiO become stronger than that for the MgNi alloy, and the intensity

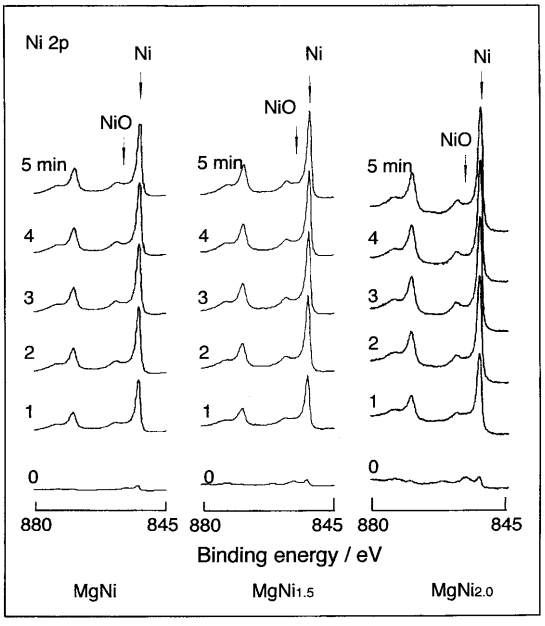


**Fig. 7** Change of Ni 2p XPS spectra of $MgNi_x$ alloys during sputtering

is dependent on the amount of Ni in the alloys, i.e., the more the Ni, the stronger the NiO peaks. Although Mg can be perfectly oxidized and Ni left in the metallic state, with the increase of Ni content in the alloys, Mg becomes insufficient to protect all the Ni at the alloy surface. Upon sputtering, the intensity of the Ni 2p peaks becomes stronger and a great increase in the amount of Ni can be clearly seen for all three alloy samples.

Figure 8 depicts the depth profiles from XPS measurements for $MgNi_x$ alloys. It can be seen that, upon sputtering, the Ni/Mg ratio changes dramatically with depth, indicating that the distribution of Mg an Ni in the alloy bulk is quite different from that on the surface. On the alloy surface, Mg dominates for all three alloys. Upon sputtering, the increase in the Ni/Mg ratio for either $MgNi_{1.5}$ or $MgNi_{2.0}$ is much more rapid than that for the MgNi alloy. The Ni/Mg ratio is 2.91 for MgNi after 4-min sputtering (corresponding a depth of about 120 Å), while is amounts to 4.34 and 4.58 for $MgNi_{1.5}$ and $MgNi_{2.0}$, respectively. The Ni/Mg ratios for both $MgNi_{1.5}$ and $MgNi_{2.0}$ are larger than that for the MgNi alloy, and similar Ni/Mg ratios were maintained between the $MgNi_{1.5}$ and $MgNi_{2.0}$ alloys. Note that the cycle performances of both $MgNi_{1.5}$ and $MgNi_{2.0}$ are much better than that of the MgNi alloy; the larger Ni/Mg ratios may be responsible for the enhancement in cycle performance of the $MgNi_{1.5}$ and $MgNi_{2.0}$ alloys.

Also from Fig. 8, it is observed that the distribution of Mg and Ni in an amorphous MgNi alloy electrode after 10 electrochemical cycles changed into the opposite of the original alloy, which indicates that the degradation of the MgNi alloy electrode involved the redistribution of Mg and Ni. This fact supports the conclusion that the Ni-enriched layer underneath the top surface of

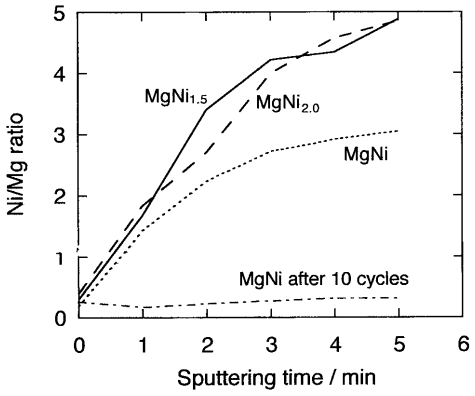


**Fig. 8** XPS depth profiles for $MgNi_x$ alloys and MgNi alloy after 20 electrochemical cycles

the alloy is responsible for the enhancement in the cycle performances of $MgNi_{1.5}$ and $MgNi_{2.0}$ alloys with respect to MgNi. The larger Ni/Mg ratio directly reflects the existence of a thicker Ni-enriched layer in the surface region of the alloys, which stabilizes the initial alloy structure during electrochemical cycling by suppressing the migration of Mg to the surface.

Figure 9 shows the atomic ratios of Ni/Mg on the top surface of the as-prepared and sputtered $MgNi_x$ alloys estimated from XPS data. The result obtained from the as-prepared alloys should correspond to the topmost surface of the alloys, and the sputtered ones should correspond to the subsurfaces. It can be seen that the Ni/Mg ratio for the subsurface of the alloys increases a great deal for both the $MgNi_{1.5}$ and $MgNi_{2.0}$ alloys as compared with the MgNi alloy, but there is no substantial difference between the $MgNi_{1.5}$ and $MgNi_{2.0}$ alloys. This fact indicates that the $MgNi_{1.5}$ and $MgNi_{2.0}$ alloys may have Ni-enriched subsurfaces with a similar thickness. The change of the Ni/Mg ratio in the top surface of the $MgNi_x$ alloys parallels very well the change in the kinetics of hydrogen absorption of the alloys, namely that the higher the Ni content in top surface of the alloy, the faster the alloy reaches its saturation capacity for hydrogen absorption. Both the top surface and the subsurface may play roles in the

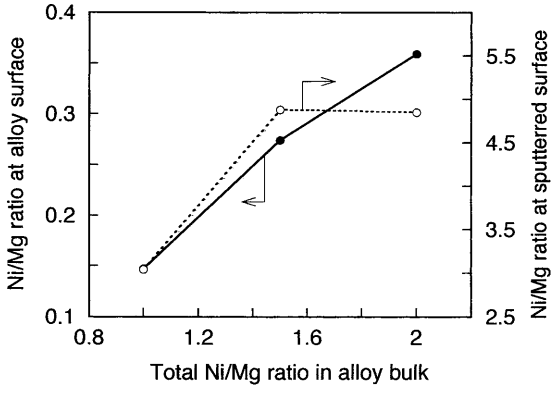


**Fig. 9** Comparison of the Ni/Mg ratio at the topmost surface with a 5-min sputtered surface of the alloys

hydrogen absorption and segregation processes of the alloy components. In the present case of $MgNi_x$, XPS analyses suggested that Ni enriched in the top surface plays a more important role than the subsurface in the hydrogen absorption process.

## Conclusion

Without any change of amorphous nature, the increase in Ni content in the alloy bulk resulted in an improvement in the hydrogen absorption kinetics of $MgNi_x$ alloys. The temperature for the $MgNi_x$ alloys to desorb hydrogen was also greatly lowered. XPS analyses indicated a change of the Ni/Mg ratio at the topmost surface strictly analogous to the change in the kinetics of hydrogen absorption for the alloys, suggesting that the Ni at the top surface plays the most important role in the hydrogen absorption processes. An inverse change in the saturation capacity with a change in the kinetics of hydrogen absorption was also observed, which revealed a probable relationship between Mg and hydrogen location in the $MgNi_x$ alloys.

The electrochemical cycle performance of $MgNi_x$ alloy electrodes can be significantly enhanced by increasing the $x$ value, i.e., introduction of excess of Ni in the alloys. XPS and XAES investigations revealed that such as effect resulted from the Ni-rich layer underneath the top surface, rather than changes in the chemical states of either Mg or Ni in the alloys. Owing to the dilution of Mg in the alloys, the discharge capacity decreased at the first cycle with the increase in Ni content.

**Acknowledgements** This work has been supported in part by Grant-in-Aid for Scientific Research on Priority Areas A of "Electrochemistry of Ordered Interfaces" no. 10131260, Grant-in-Aid for Scientific Research on Priority Areas A of "New Protium Function" no. 10148105, Grant-in-Aid for Scientific Research (B) no. 09555273, and Grant-in-Aid for "Encouragement of Young Scientists" no. 10750602 from the Ministry of Education, Science, Sports and Culture of Japan.

## References

1. Dillon AC, Jones KM, Bekkedahl TA, Kiang CH, Bethune DS, Heben MJ (1997) Nature 386: 377
2. Chambers A, Park C, Baker RTK, Rodriguez NM (1998) J Phys Chem B 102: 4253
3. Reilly JJ, Wiswall RH (1968) Inorg Chem 7: 2254
4. Lei YQ, Wu YM, Yang QM, Wu J, Wang QD (1994) Z Phys Chem B 183: 379
5. Iwakura C, Nohara S, Inoue H, Fukumoto Y (1996) J Chem Soc Chem Commun 1831
6. Orimo S, Fujii H (1997) J Alloys Compd 232: L16
7. Kohno T, Kanda M (1997) J Electrochem Soc 144: 2343
8. Nohara S, Fujita N, Zhang SG, Inoue H, Iwakura C (1998) J Alloys Compd 267: 76
9. Iwakura C, Inoue H, Zhang SG, Nohara S (1998) J Alloys Compd 270: 142
10. Nohara S, Hamasaki K, Zhang SG, Inoue H, Iwakura C (1998) J Alloys Compd 280: 104
11. Orimo S, Ikeda K, Fujii H, Yamamoto K (1997) J Alloys Compd 260: 143
12. Sakuguchi H, Seri H, Adachi G (1990) J Phys Chem 94: 5313
13. Hansen J (1958) Constitution of binary alloys. McGraw-Hill, New York
14. Iwakura C, Inoue H, Zhang SG, Nohara S, Yorimitsu K, Kuramoto N, Morikawa T (1999) J Electrochem Soc 146: 1659
15. Zhang SG, Yorimitsu K, Morikawa T, Nohara S, Inoue H, Iwakura C (1998) J Alloys Compd 270: 123
16. Nohara S, Inoue H, Fukumoto Y, Iwakura C (1997) J Alloys Compd 259: 183
17. Stepanov A, Ivanov E, Konstachuk I, Boldyrev V (1987) J Less-Common Met 131: 89
18. Wagner CD, Biloen P (1973) Surf Sci 35: 82
19. Kim KS, Winograd N (1970) Surf Sci 43: 625